

Article

Mechanistic Insights into Selective Hydrogenation of C=C Bonds Catalyzed by CCC Cobalt Pincer Complexes: A DFT Study

Zheng Zuo^{1,2,3} and Xinzheng Yang^{1,2,3,*} 

¹ State Key Laboratory for Structural Chemistry of Unstable and Stable Species, Institute of Chemistry Chinese Academy of Sciences, Beijing 100190, China; zzwll@iccas.ac.cn

² University of Chinese Academy of Sciences, Beijing 100049, China

³ Beijing National Laboratory for Molecular Sciences, CAS Research/Education Center for Excellence in Molecular Sciences, Beijing 100190, China

* Correspondence: xyang@iccas.ac.cn

Abstract: The mechanistic insights into hydrogenations of hex-5-en-2-one, isoprene, and 4-vinylcyclohex-1-ene catalyzed by pincer (^{Mes}CCC)Co (Mes = bis(mesityl-benzimidazol-2-ylidene)phenyl) complexes are computationally investigated by using the density functional theory. Different from a previously proposed mechanism with a cobalt dihydrogen complex (^{Mes}CCC)Co-H₂ as the catalyst, we found that its less stable dihydride isomer, (^{Mes}CCC)Co(H)₂, is the real catalyst in those catalytic cycles. The generations of final products with H₂ cleavages for the formations of C–H bonds are the turnover-limiting steps in all three hydrogenation reactions. We found that the hydrogenation selectivity of different C=C bonds in the same compound is dominated by the steric effects, while the hydrogenation selectivity of C=C and C=O bonds in the same compound could be primarily influenced by the electronic effects. In addition, the observed inhibition of the hydrogenation reactions by excessive addition of PPh₃ could be explained by a 15.8 kcal/mol free energy barrier for the dissociation of PPh₃ from the precatalyst.



Citation: Zuo, Z.; Yang, X. Mechanistic Insights into Selective Hydrogenation of C=C Bonds Catalyzed by CCC Cobalt Pincer Complexes: A DFT Study. *Catalysts* **2021**, *11*, 168. <https://doi.org/10.3390/catal11020168>

Received: 3 January 2021

Accepted: 20 January 2021

Published: 26 January 2021

Publisher's Note: MDPI stays neutral with regard to jurisdictional claims in published maps and institutional affiliations.



Copyright: © 2021 by the authors. Licensee MDPI, Basel, Switzerland. This article is an open access article distributed under the terms and conditions of the Creative Commons Attribution (CC BY) license (<https://creativecommons.org/licenses/by/4.0/>).

Keywords: hydrogenation; homogeneous catalysis; catalytic mechanism; cobalt pincer complex; density functional theory

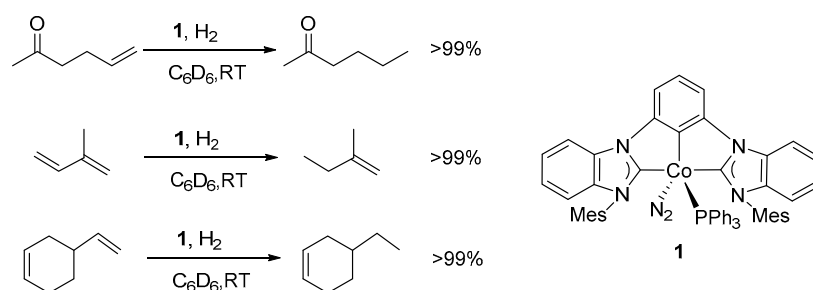
1. Introduction

The selective hydrogenation of functionalized alkenes remains a largely unmet need in petrochemical, fine chemical, and pharmaceutical industries [1–5]. Homogeneously catalytic hydrogenation is one of the most atom economical methods for the hydrogenation of functionalized alkenes [6]. For nearly half a century, most reported catalysts for hydrogenation reactions relied principally on expensive and toxic noble metals, such as Ir [7], Rh [8,9], Ru [10–12], etc. [13,14]. The environmental impact and high cost of those scarce elements are driving people to develop more cost-effective and environmentally benign catalysts based on earth-abundant metals, such as iron and cobalt [15]. Although some progress has been achieved in iron-catalyzed (de)hydrogenation reactions at ambient temperatures and pressures [16–20], only a few Co catalysts for alkene hydrogenation reactions have been reported so far [21–29].

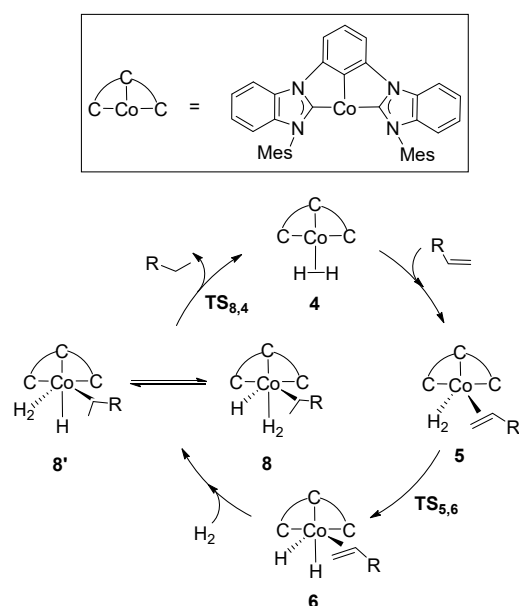
In 2004, Budzelaar and co-workers [21] developed Co pincer complexes LCoR (L = 2,6-[RN=CMe]₂C₅H₃N; R = *n*-C₆H₁₃ or 2,6-(*i*-Pr)₂C₆H₃) for the catalytic hydrogenation of monosubstituted olefins under 50 °C and 20 atm pressure. They found that reducing the steric bulk at the imine positions and changing the metal from cobalt to rhodium did not change catalytic activities much. Such results indicated that cobalt complexes could be “rhodium-like” catalysts with proper ligands. In 2012, Hanson and co-workers [22] reported a versatile Co(II) alkyl complex for the catalytic hydrogenation of olefins, ketones,

aldehydes, and imines with yields of up to 90% under mild conditions. They also developed a cationic Co(II) alkyl complex as an effective precatalyst for the dehydrogenation of alcohols and hydrogenation of olefins and ketones with high yields (>95%) under mild conditions (25 °C, 1 atm H₂) [23]. Their experimental studies suggested that the olefin hydrogenation reaction underwent an insertion mechanism with a Co(II) hydride complex as the catalyst, while the alcohol dehydrogenation reaction proceeded through a Co(I)/(III) redox catalytic cycle. Later on, Peters and co-workers [24,25] found bis-(phosphino)boryl cobalt complexes as catalysts for C=C bond hydrogenations with high yields (>95%) at room temperature and 1 atm H₂ pressure. Their kinetic studies indicated that the turnover-limiting step involved a binuclear cobalt complex. In 2015, Chirik and co-workers [26] developed a bis(imino)pyridine cobalt complex for the catalytic hydrogenation of substituted benzofused five-, six-, and seven-membered alkenes with high yields (>95%) and enantioselectivities (>95% *ee*) under mild conditions (25 °C and 4 atm H₂). They also found that both the ring size and *exo/endo* disposition affected the stereochemistry.

Fout and co-workers [27] recently developed a series of cobalt catalysts with electron-rich monoanionic bis(carbene) ligands, ^{Mes}CCC (bis(mesityl-benzimidazol-2-ylidene)phenyl) and ^{DIPP}CCC (bis(diisopropylphenyl-benzimidazol-2-ylidene)phenyl), for the rapid and highly chemoselective hydrogenation of olefins (Scheme 1). They found the viability of Co^I/Co^{III} redox cycles in such olefin hydrogenation reactions and proposed a plausible mechanism with a cobalt dihydrogen complex (^{Mes}CCC)Co-H₂ as the catalyst (Scheme 2) [27]. In the proposed mechanism, a reactant molecule fills the vacant position in **4** and forms intermediate **5**. The oxidative addition of H₂ in **5** forms a dihydride complex **6**. When another H₂ approaches **6**, **8** and **8'** could be formed through H₂ cleavage and C–H bond formation. Then, the product is formed and the catalyst **4** is regenerated with the formation of another C–H bond. Their following experimental studies indicated the existence of cobalt-alkyl hydride complex generating (**5** → **6**) and β-H elimination (**8** → **6**) steps [28]. They also extended the application of (^{Mes}CCC)Co complexes for the catalytic semihydrogenation of alkynes and found the generation of *E*-selective products from a wide range of alkynes with yields of up to 80% and a *E/Z* selectivity over 99% [29]. Furthermore, Fout and co-workers [30] studied the electronic modification effect of ^{Mes}CCC^R pincer ligands and found that the *tert*-butyl group did not affect the reactivity, while the CF₃ group changed the product ratios. Although a plausible catalytic cycle has been proposed, the mechanistic insights into the above (^{Mes}CCC)Co catalyzed hydrogenation reactions, especially the origin of high chemo-selectivities, still remain unclear. Herein, we computationally investigated detailed mechanisms of the hydrogenation reactions of hex-5-en-2-one, isoprene, and 4-vinylcyclohex-1-ene catalyzed by (^{Mes}CCC)Co using the density functional theory (DFT), analyzed the causes of selectivities in hydrogenations of C=C and C=O bonds, as well as the C=C bonds in the same compounds, and explained why the addition of excessive PPh₃ ligands inhibited the reactions.



Scheme 1. High chemoselectivities for the hydrogenation of olefins catalyzed by Fout and co-workers' (^{Mes}CCC)Co complexes.



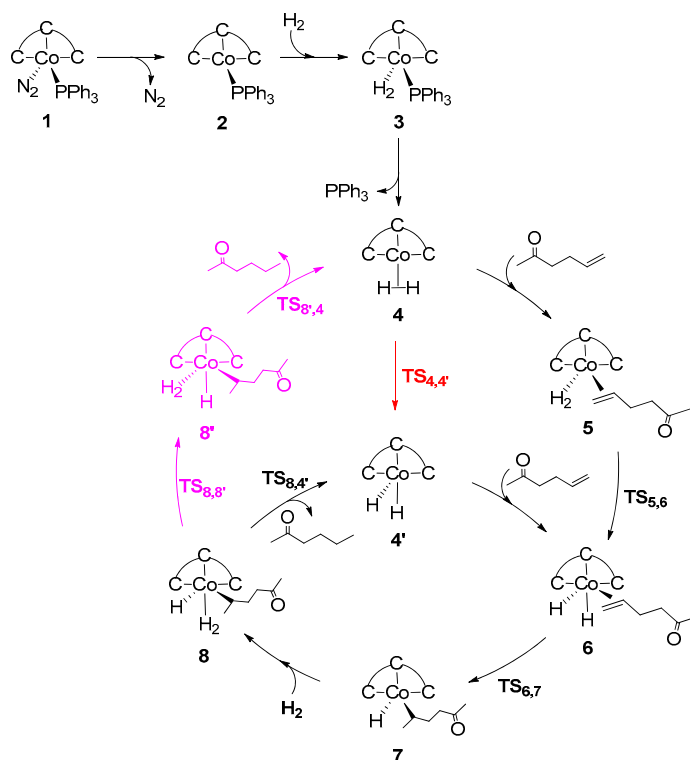
Scheme 2. Fout and co-workers' plausible mechanism of the hydrogenation of alkenes catalyzed by $(\text{MesCCC})\text{Co}$ complexes.

2. Results and Discussion

2.1. Hydrogenation of Hex-5-En-2-One

2.1.1. Hydrogenation of C=C Bond

The predicted catalytic cycle and the corresponding free energy profile for the hydrogenation of hex-5-en-2-one to hexan-2-one are shown in Scheme 3 and Figure 1, respectively. The optimized structures of key transition states in this reaction are displayed in Figure 2.



Scheme 3. Proposed catalytic cycle for the hydrogenation of hex-5-en-2-one to hexan-2-one catalyzed by $(\text{MesCCC})\text{Co}$ complexes.

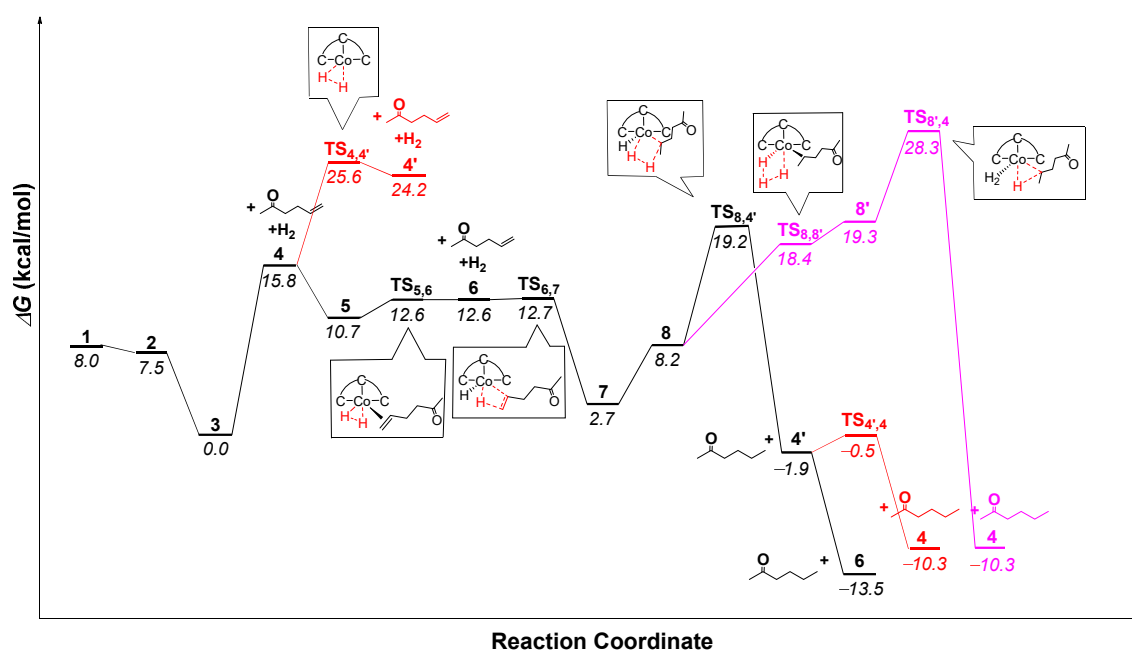


Figure 1. Free energy profile for the hydrogenation of hex-5-en-2-one to hexan-2-one catalyzed by $(\text{Mes}^3\text{CC})\text{Co}$ complexes.

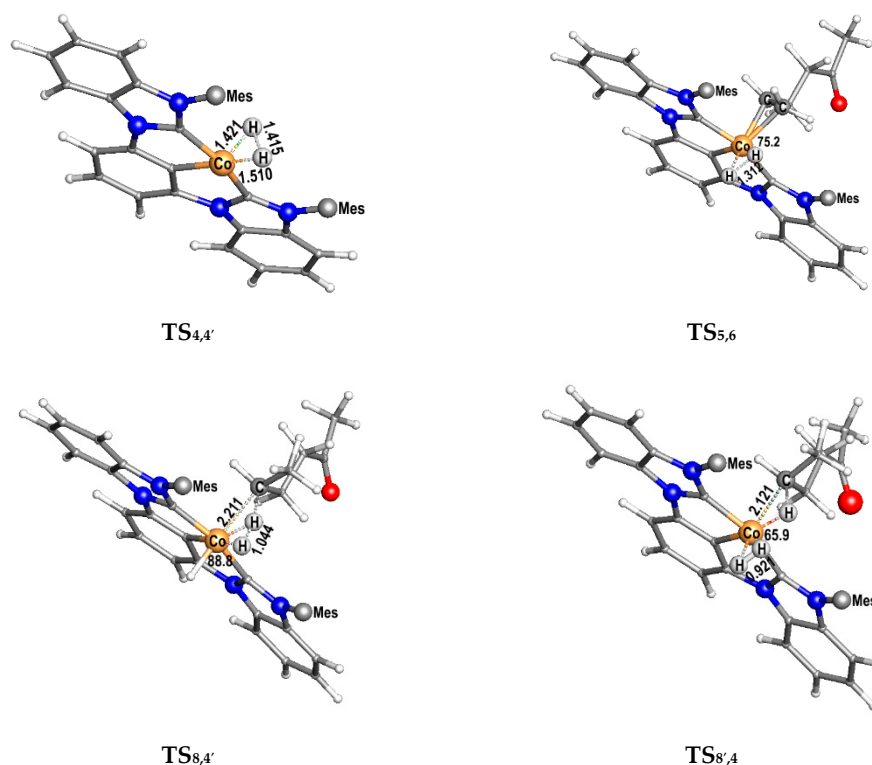


Figure 2. Optimized structures of $\text{TS}_{4,4'}$ ($664i\text{ cm}^{-1}$), $\text{TS}_{5,6}$ ($742i\text{ cm}^{-1}$), $\text{TS}_{8,4'}$ ($1068i\text{ cm}^{-1}$), and $\text{TS}_{8',4}$ ($838i\text{ cm}^{-1}$). Mesitylene groups are omitted for clarity. Bond lengths are in Å, and bond angles are in $^\circ$.

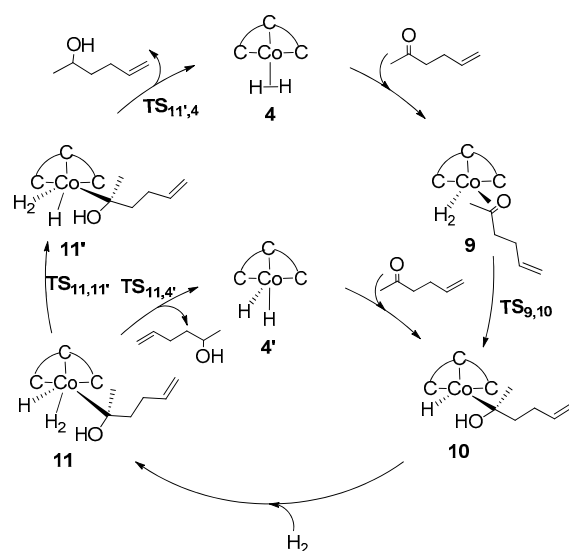
At the beginning of the reaction, a H_2 molecule replaces the N_2 in **1** and forms an 8.0-kcal/mol more stable intermediate **3**. The dissociation of PPh_3 from **3** is a 15.8-kcal/mol uphill step. The dihydrogen complex $(\text{Mes}^3\text{CC})\text{Co-H}_2$ (**4**) was considered as the catalyst in a previous study [27]. Once **4** is formed, a hex-5-en-2-one molecule can easily coordinate to **4** with its $\text{C}=\text{C}$ bond and form a 5.1-kcal/mol more stable intermediate **5**. The oxidative addition of H_2 in **5** has a very low barrier of 1.9 kcal/mol ($\text{TS}_{5,6}$). Such a low barrier

indicates that the transformation between **5** and **6** is reversible, which corresponds to the experiments. Then, a hydride in **6** can easily transfer from cobalt to the end carbon atom in the coordinated C=C bond via $\text{TS}_{6,7}$ and form a more stable intermediate **7**. Another H_2 molecule can coordinate to **7** and form a 5.5-kcal/mol less stable complex **8**.

There are two ways for the cleavage of H_2 in **8** to occur. One is a proton transfer from H_2 to the carbon bonding to Co via $\text{TS}_{8,4'}$ with a free energy barrier of 19.2 kcal/mol. A stable dihydride complex **4'** is formed with the dissociation of hex-2-one. **4'** could attract a hex-5-en-2-one molecule and complete a catalytic cycle with the formation of **6**. The other way for H_2 cleavage to occur is a proton transfer from H_2 to the hydride bonding to Co for the formation of **8'**, which is an 11.1-kcal/mol less stable isomer of **8** with rearranged hydrogen atoms. Then, a hex-2-one molecule is formed through reductive elimination ($\text{TS}_{8',4}$), which is 9.1-kcal/mol higher than $\text{TS}_{8,4'}$ in free energy and unlikely to happen in the reaction. Therefore, the dihydride complex **4'** is believed to be the more reasonable catalyst for the hydrogenation of hex-5-en-2-one, with a total free energy barrier of 19.2 kcal/mol (**3** \rightarrow $\text{TS}_{8,4'}$). It is worth noting that the slightly lower free energy of $\text{TS}_{8,8'}$ than **8'** is caused by thermal corrections. We can consider that this does not practically exist at the experimental temperature.

2.1.2. Hydrogenation of C=O Bond

The reaction cycle and corresponding free energy profile for the hydrogenation of hex-5-en-2-one to hex-5-en-2-ol are shown in Scheme 4 and Figure 3, respectively. The optimized structures of key intermediates and transition states in this cycle are displayed in Figure 4. After the formation of **4**, the coordination of the C=O bond in hex-5-en-2-one to Co forms a 7.1-kcal/mol less stable intermediate **9**. We believe that this is primarily caused by the methyl and butene groups on carbonyl, which prevent the end-on bonding of carbonyl to Co and make the coordination of C=O much weaker than the Dewar–Chatt–Duncanson (DCD) model bonding between C=C and Co. In addition, the methyl group on carbonyl also increases the difficulty of C=O bonding to Co. After the formation of **9**, the oxygen atom in hex-5-en-2-one could assist H_2 splitting for the formation of an O–H bond in **10** with a free energy barrier of 41.3 kcal mol⁻¹ ($\text{TS}_{9,10}$). Then, the complex **11** is formed with the coordination of another H_2 molecule. Like **8** in the C=C bond hydrogenation mechanism shown in Scheme 3, **11** is the bifurcating point in the reaction cycle for C=O bond hydrogenation. The free energy profile in Figure 3 indicates that the formation of hex-5-en-2-ol by simultaneous H_2 cleavage and C–H bond formation via $\text{TS}_{11,4'}$ is 8.8 kcal/mol lower than $\text{TS}_{11,4}$. Therefore, $\text{TS}_{11,4'}$ is the rate-determining step in the reaction with a total free energy barrier of 44.1 kcal/mol (**3** \rightarrow $\text{TS}_{11,4'}$) for the formation of hex-5-en-2-ol. Such a high barrier indicates that (^{Mes}CCC)Co cannot catalyze the hydrogenation of the C=O bond in hex-5-en-2-one. The oxygen atom in $\text{TS}_{11,4'}$ decreases the electron density of carbon atom bonding to Co. The low electron density of the carbon atom makes it hard for the $\text{TS}_{11,4'}$ step to happen. Such a reason may explain the selectivity of the hydrogenation of C=C and C=O bonds in a compound.



Scheme 4. Proposed catalytic cycle for the hydrogenation of hex-5-en-2-one to hex-5-en-2-ol catalyzed by $(^{\text{Mes}}\text{CCC})\text{Co}$ complexes.

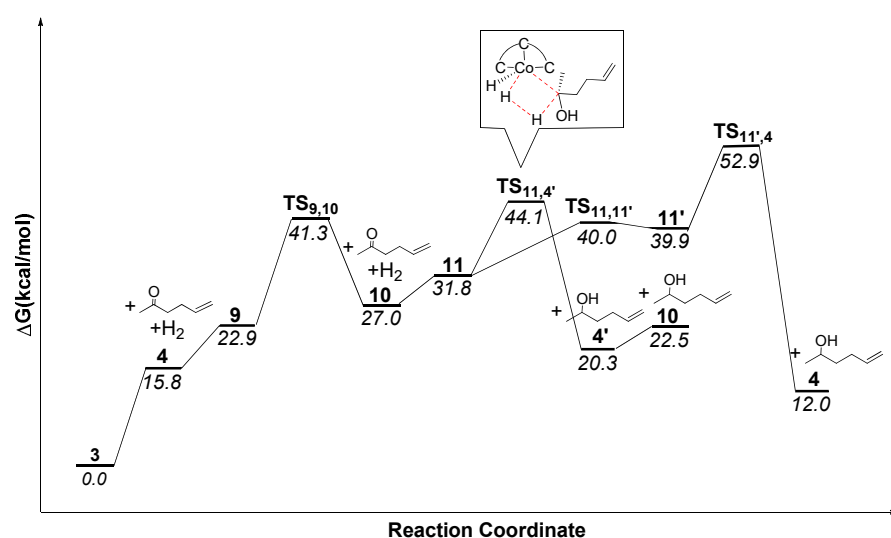


Figure 3. Free energy profile for the hydrogenation of hex-5-en-2-one to hex-5-en-2-ol catalyzed by $(^{\text{Mes}}\text{CCC})\text{Co}$ complexes.

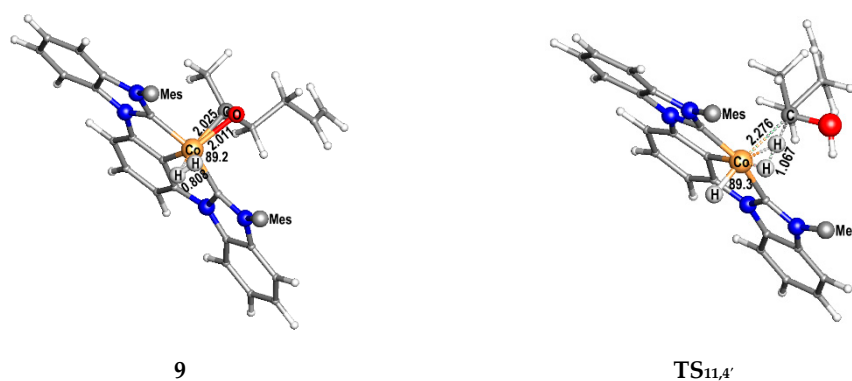
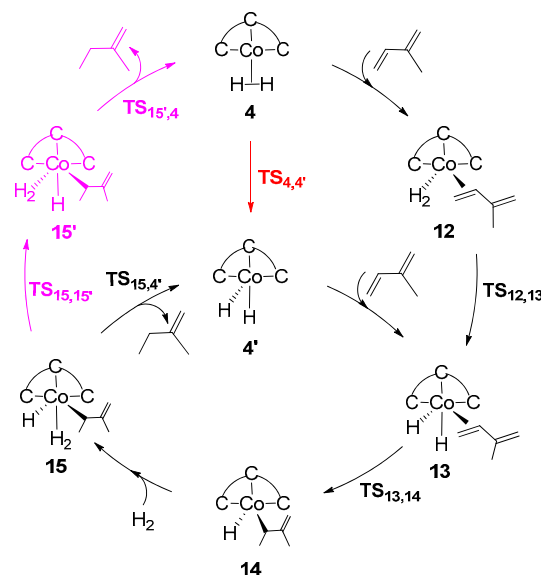


Figure 4. Optimized structures of **9** and **TS_{11,4'}** ($1095i\text{ cm}^{-1}$). Mesitylene groups are omitted for clarity. Bond lengths are in Å, and bond angles are in °.

2.2. Hydrogenation of Isoprene

2.2.1. Hydrogenation of Singly Substituted C=C Double Bond

The predicted catalytic cycle and the corresponding free energy profile for the hydrogenation of isoprene to 2-methylbut-1-ene are shown in Scheme 5 and Figure 5, respectively. The optimized structures of key intermediates and transition states in this reaction are displayed in Figure 6.



Scheme 5. Proposed catalytic cycle for the hydrogenation of isoprene to 2-methylbut-1-ene catalyzed by $(\text{Mes}^3\text{CCC})\text{Co}$ complexes.

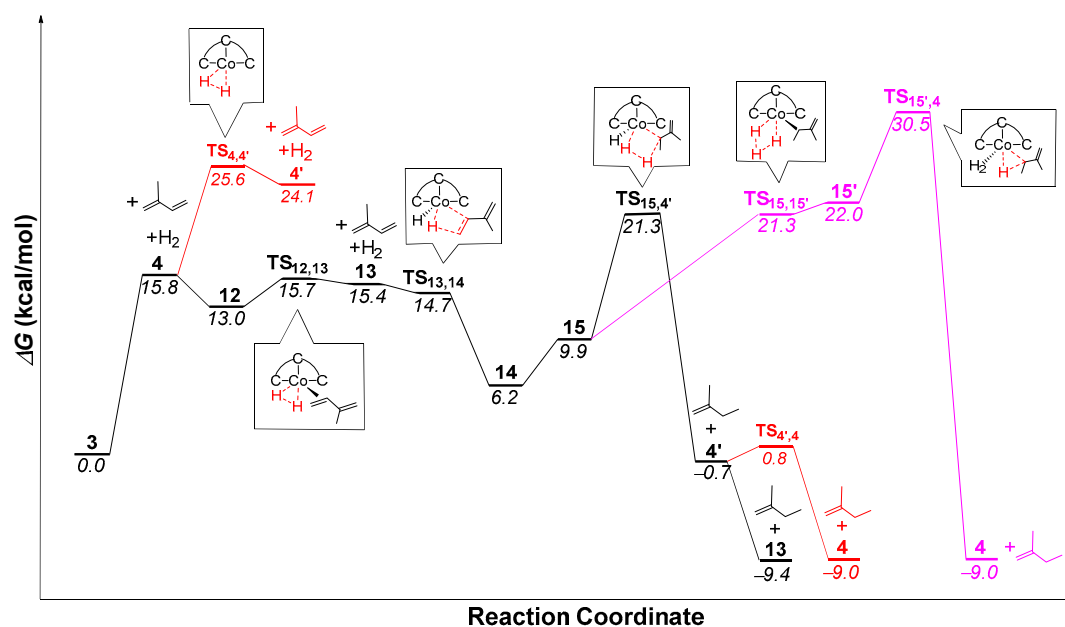


Figure 5. Free energy profile for the hydrogenation of isoprene to 2-methylbut-1-ene catalyzed by $(\text{Mes}^3\text{CCC})\text{Co}$ complexes.

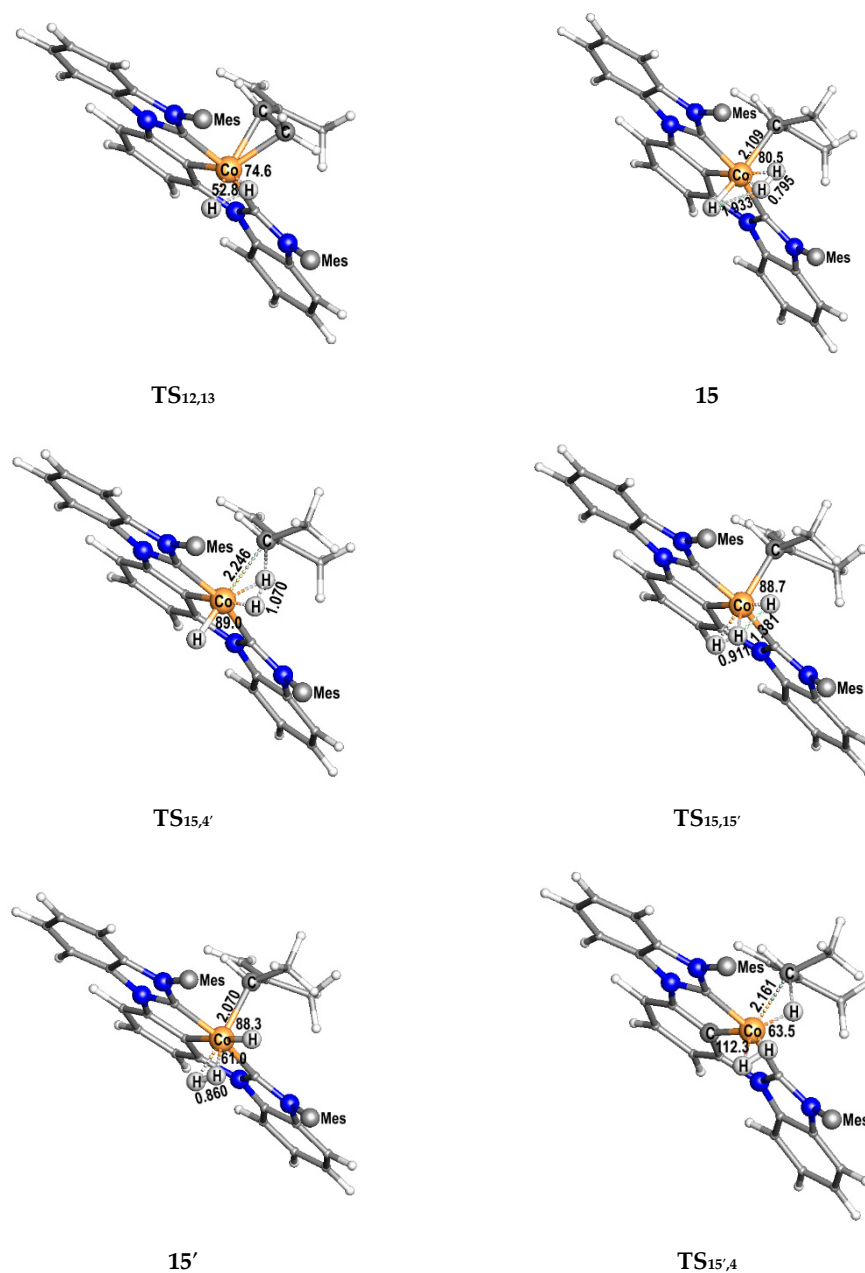


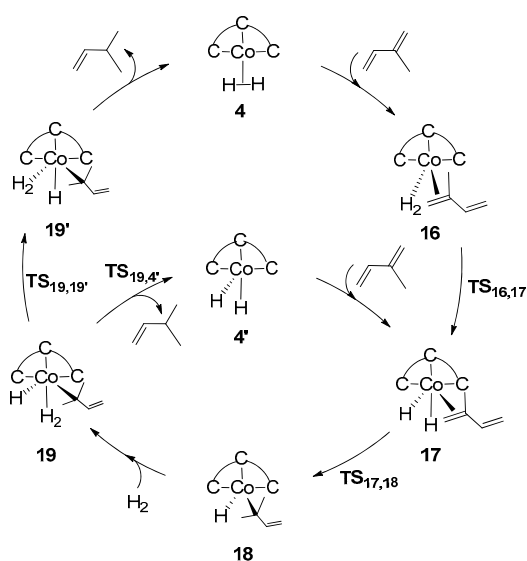
Figure 6. Optimized structures of $\text{TS}_{12,13}$ ($722i\text{ cm}^{-1}$), **15**, $\text{TS}_{15,4'}$ ($1148i\text{ cm}^{-1}$), $\text{TS}_{15,15'}$ ($340i\text{ cm}^{-1}$), **15'**, and $\text{TS}_{15,4}$ ($932i\text{ cm}^{-1}$). Mesitylene groups are omitted for clarity. Bond lengths are in Å, and bond angles are in °.

Once **4** is formed, a singly substituted C=C bond in an isoprene molecule can coordinate to **4** and form a 2.8-kcal/mol more stable intermediate **12** with a DCD model bonding. The oxidative addition of H_2 in **12** for the formation of the dihydride complex **13** has a rather low barrier of 2.7 kcal/mol ($\text{TS}_{12,13}$). Such a low barrier indicates that the transformation between **12** and **13** is reversible, which corresponds to the experiments. After the H_2 cleavage, a hydrogen can easily transfer from cobalt to the end carbon atom in the coordinated C=C bond via $\text{TS}_{13,14}$ and form the intermediate **14**, which is 9.6 kcal/mol more stable than **4**. Then, another H_2 molecule comes in for the formation of **15**, which is the bifurcating point in this catalytic reaction. The formation of 2-methylbut-1-ene with the transfer of a proton from H_2 to the coordinated carbon atom via $\text{TS}_{15,4'}$ is 9.2-kcal/mol more favorable than $\text{TS}_{15',4}$. Therefore, we believe that $\text{TS}_{15,4'}$ is the rate-determining step

for the hydrogenation of isoprene with a total free energy barrier of 21.3 kcal/mol ($3 \rightarrow \text{TS}_{15,4'}$).

2.2.2. Hydrogenation of the Doubly Substituted C=C Double Bond

In order to find out the key factors that influence the selectivity of different C=C bonds, we also studied the mechanism for the hydrogenation of the doubly substituted C=C bond in isoprene. The reaction cycle and corresponding free energy profile for the hydrogenation of isoprene to 3-methylbut-1-ene are shown in Scheme 6 and Figure 7, respectively. The optimized structures of key intermediates and transition states in this cycle are displayed in Figure 8.



Scheme 6. Proposed catalytic cycle for the hydrogenation of isoprene to 3-methylbut-1-ene catalyzed by $(\text{Mes}^3\text{CC})\text{Co}$ complexes.

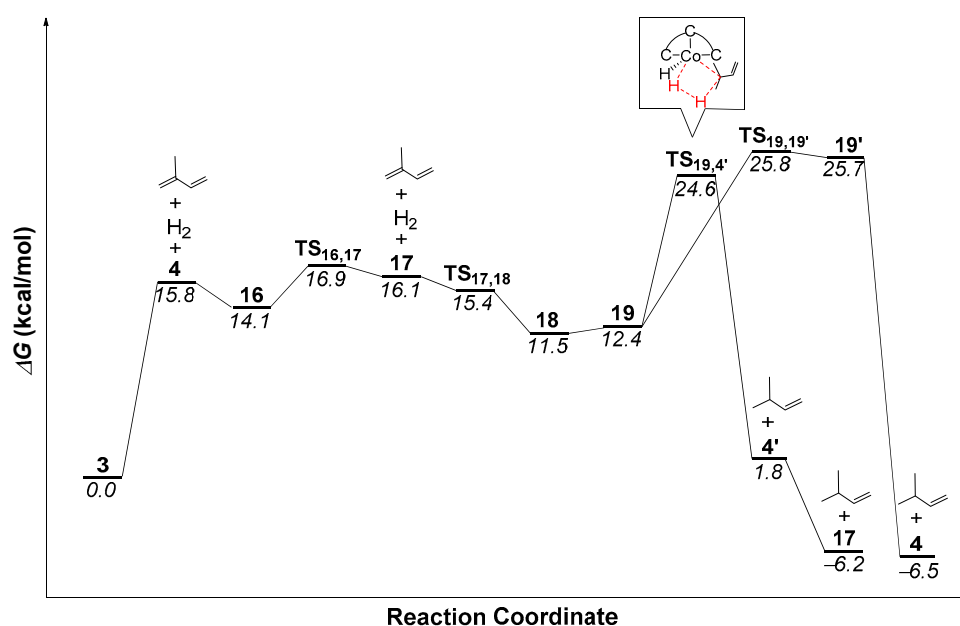


Figure 7. Free energy profile for the hydrogenation of isoprene to 3-methylbut-1-ene catalyzed by $(\text{Mes}^3\text{CC})\text{Co}$ complexes.

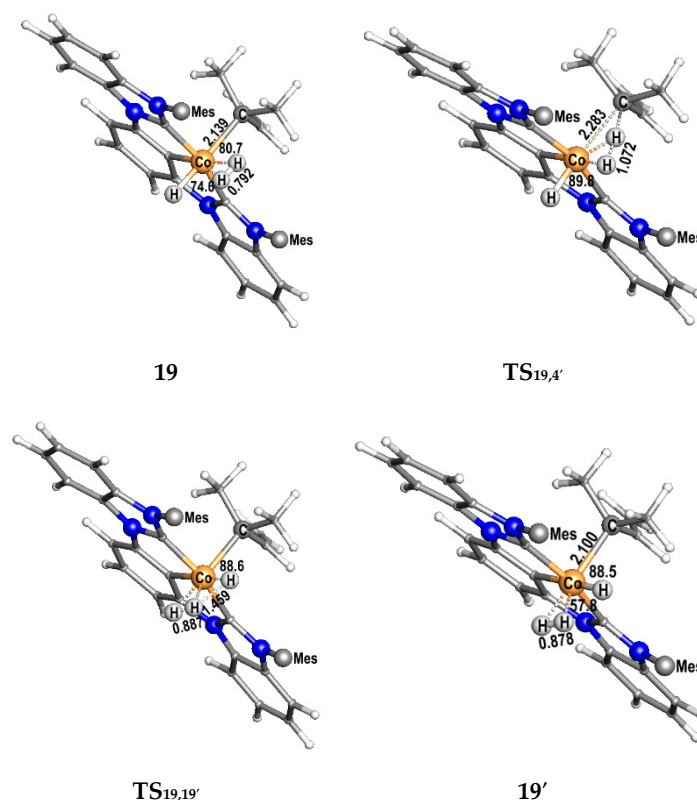


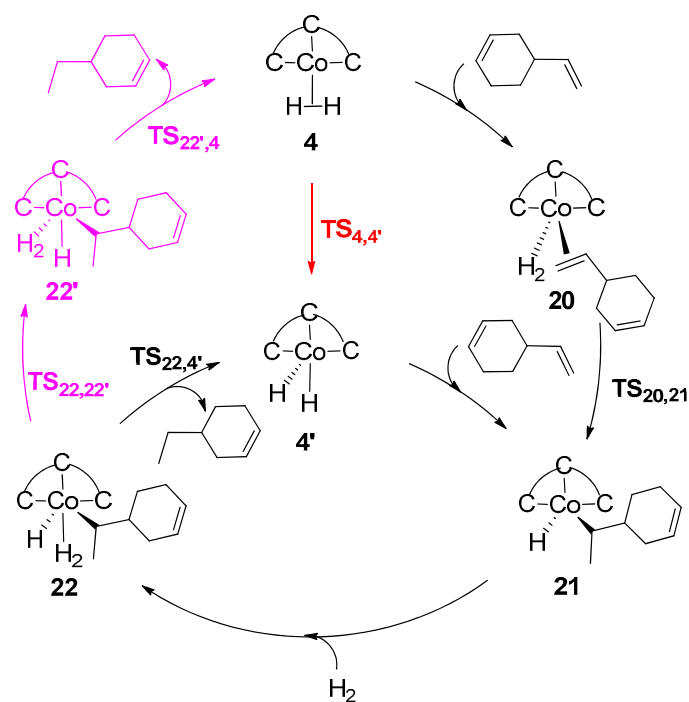
Figure 8. Optimized structures of **19**, **TS_{19,4'}** (1150i cm⁻¹), **TS_{19,19'}** (129i cm⁻¹), and **19'**. Mesitylene groups are omitted for clarity. Bond lengths are in Å, and bond angles are in °.

The formation of 3-methylbut-1-ene has a similar pathway as the hydrogenations of hex-5-en-2-one and isoprene, but slightly different relative free energies. Because of the bulky structures of mesitylene groups in the CCC ligand, the coordination of the doubly substituted C=C bond to Co is 1.1-kcal/mol less favorable than the coordination of the singly substituted C=C bond in isoprene. Complex **19** is the bifurcating point in this reaction, while the H₂ cleavage for the formation of 3-methylbut-1-ene is the turnover-limiting step with a total free energy barrier of 24.6 kcal/mol (**3** → **TS_{19,4'}**), which is 3.3 kcal/mol higher than the barrier for the formation of 2-methylbut-1-ene (Figure 5). Such a high barrier indicates that (^{Mes}CCC)Co cannot catalyze the hydrogenation of the doubly substituted C=C bond in isoprene because the steric effect between the doubly substituted C=C bond and (^{Mes}CCC)Co is larger than that of singly substituted C=C bonds. The distance between C(CH₃)₂-CH=CH₂ and H₂ bonding to Co in **TS_{19,4'}** is larger than that between CH(CH₃)-C(CH₃)=CH₂ and H₂ bonding to Co in **TS_{15,4'}**; the large distance makes it hard for the **TS_{19,4'}** step to happen. Such a reason may explain the selectivity of the hydrogenation.

2.3. Hydrogenation of 4-Vinylcyclohex-1-Ene

2.3.1. Hydrogenation of the Exocycle C=C Bond

In order to find out the key factors that influence the selectivity in the hydrogenation of the C=C bond in cycloalkene derivatives, we further explored the mechanism for the hydrogenation of 4-vinylcyclohex-1-ene to 4-ethylcyclohex-1-ene. The predicted catalytic cycle and the corresponding free energy profile are shown in Scheme 7 and Figure 9, respectively. The optimized structures of key intermediates and transition states are displayed in Figure 10.



Scheme 7. Proposed catalytic cycle for the hydrogenation of 4-vinylcyclohex-1-ene to 4-ethylcyclohex-1-ene catalyzed by $(^{\text{Mes}}\text{CCC})\text{Co}$ complexes.

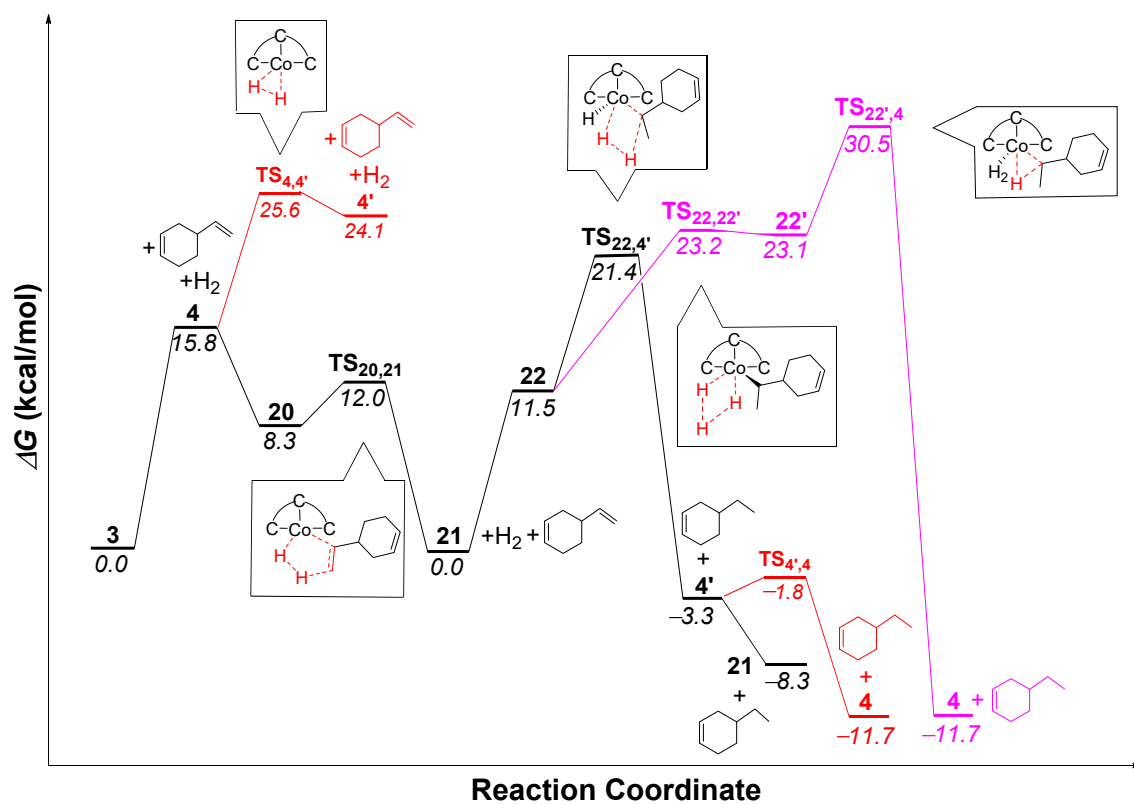


Figure 9. Free energy profile for the hydrogenation of 4-vinylcyclohex-1-ene to 4-ethylcyclohex-1-ene catalyzed by $(^{\text{Mes}}\text{CCC})\text{Co}$ complexes.

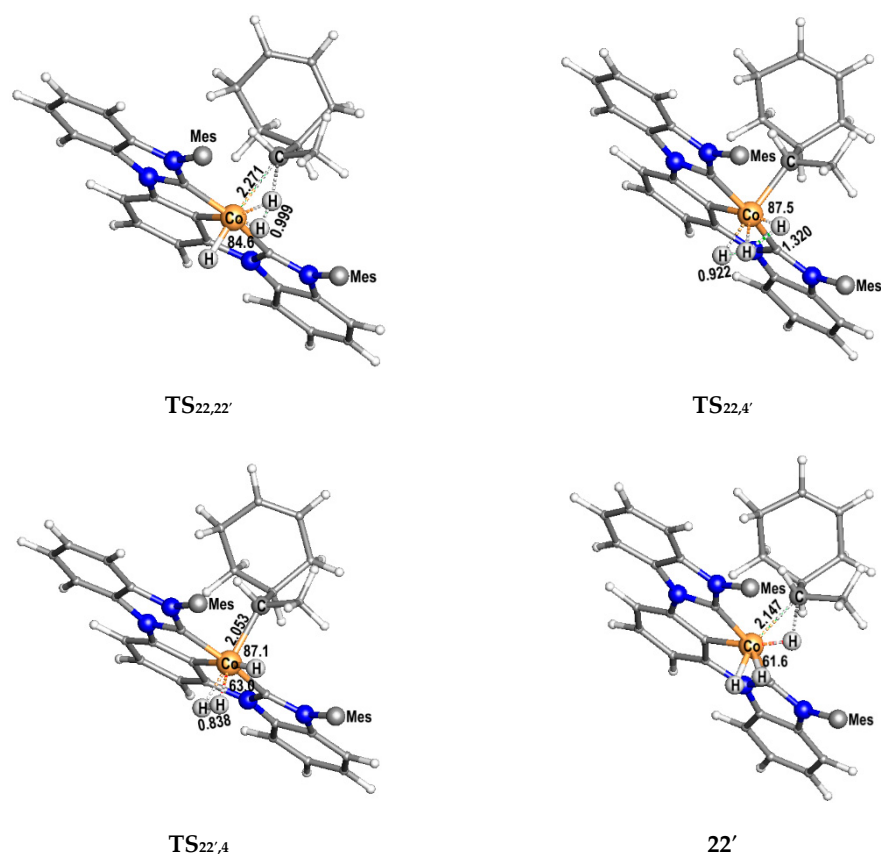


Figure 10. Optimized structures of $\text{TS}_{22,4'}$ ($927i\text{ cm}^{-1}$), $\text{TS}_{22,22'}$ ($502i\text{ cm}^{-1}$), $22'$, and $\text{TS}_{22',4}$ ($775i\text{ cm}^{-1}$). Mesitylene groups are omitted for clarity. Bond lengths are in Å, and bond angles are in $^\circ$.

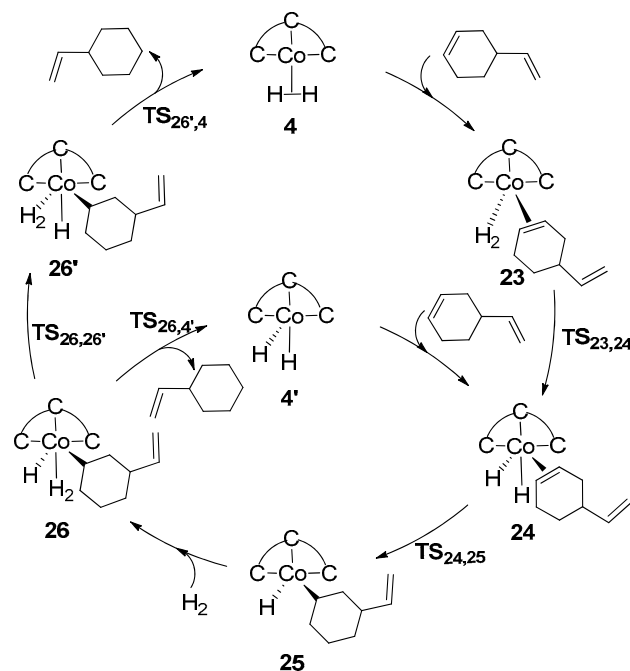
After the formation of **4**, a 4-vinylcyclohex-1-ene molecule coordinates to **4** with its C=C double bond at the exocycle and forms a 7.5-kcal/mol more stable intermediate **20**. The following H_2 cleavage and hydrogenation process for the formation of 4-ethylcyclohex-1-ene are similar to the above pathways in the hydrogenations of hex-5-en-2-one and isoprene. **22** is the bifurcating point of the reaction, like **8** in the hydrogenation of the C=C bond in hex-5-en-2-one. The calculated free energy profile indicates that the formation of 4-ethylcyclohex-1-ene with the cleavage of H_2 ($\text{TS}_{22,4'}$) is the turnover-limiting step in this reaction. **4'** is believed to be the more reasonable catalyst for the hydrogenation of 4-vinylcyclohex-1-ene with a total free energy barrier of 21.4 kcal/mol ($3 \rightarrow \text{TS}_{22,4'}$).

2.3.2. Hydrogenation of the C=C Bond in Cycle

The reaction cycle and corresponding free energy profile for the hydrogenation of 4-vinylcyclohex-1-ene to vinylcyclohexane are shown in Scheme 8 and Figure 11, respectively. The optimized structures of key intermediates and transition states are displayed in Figure 12.

Because of the bulky structures of cyclohexene in the 4-vinylcyclohex-1-ene and mesitylene groups in the CCC ligand, the coordination of the C=C bond in cyclohexene to Co forms a 4.7-kcal/mol less stable intermediate **23**. Although the formations of vinylcyclohexane and 4-ethylcyclohex-1-ene have similar reaction pathways, their energy profiles are different. As shown in Figure 11, the turnover-limiting step $\text{TS}_{26,4'}$ has a total free energy barrier of 29.9 kcal/mol ($3 \rightarrow \text{TS}_{26,4'}$), which is 8.5 kcal/mol higher than the barrier for the formation of 4-ethylcyclohex-1-ene. Such a high barrier indicates that $(^{\text{Mes}}\text{CCC})\text{Co}$ cannot catalyze the hydrogenation of the C=C bond in the cyclohexene of 4-vinylcyclohex-1-ene because the steric effect between the C=C bond in cyclohexene and $(^{\text{Mes}}\text{CCC})\text{Co}$ is larger than that of the exocycle C=C bond. The distance between the C atom in cyclohexene

and H₂ bonding to Co in TS_{26,4'} is larger than that between the C atom in chain and H₂ bonding to Co in TS_{22,4'}; the large distance makes it hard for the TS_{26,4'} step to happen. Such a reason may explain the selectivity of the hydrogenation.



Scheme 8. Proposed catalytic cycle for the hydrogenation of 4-vinylcyclohex-1-ene to vinylcyclohexane catalyzed by (Mes³CC)Co complexes.

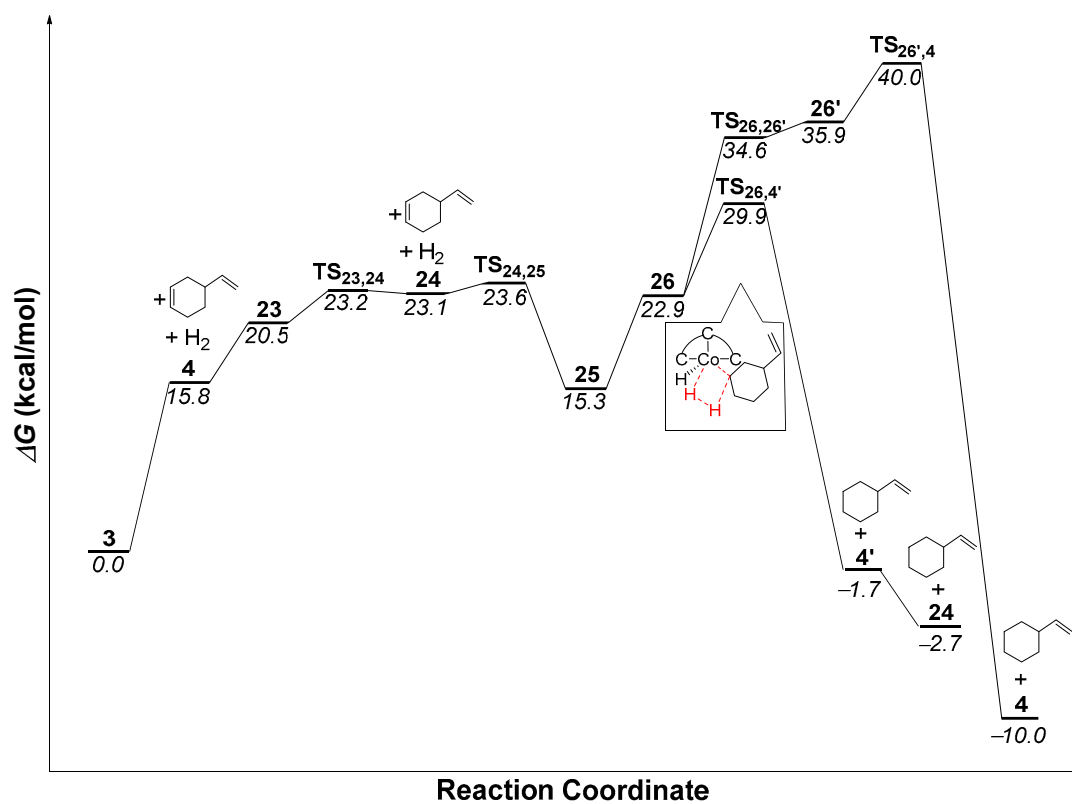


Figure 11. Free energy profile for the hydrogenation of 4-vinylcyclohex-1-ene to vinylcyclohexane catalyzed by (Mes³CC)Co complexes.

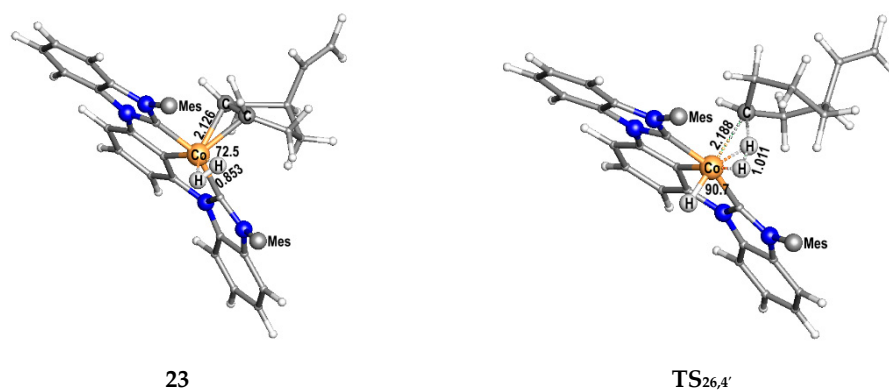


Figure 12. Optimized structures of **23** and $\text{TS}_{26,4'}$ ($1033i \text{ cm}^{-1}$). Mesitylene groups are omitted for clarity. Bond lengths are in Å, and bond angles are in $^\circ$.

3. Computational Details

All DFT calculations in this study were executed using the Gaussian 09 programs package [31] for the $\omega\text{B97X-D}$ functional [32]. The all-electron 6-31G(d,p) basis set was used for H, C, O, N, and P atoms [33,34], while the Stuttgart relativistic effective core potential basis set (ECP10MDF) was used for Co [35]. All structures were optimized with solvent effect corrections using the integral equation formalism polarizable continuum model (IEFPCM) [36] with the SMD (solvation model based on the quantum mechanical charge density) [37] variation for benzene. Thermal corrections were calculated within the harmonic potential approximation under $T = 298.15 \text{ K}$ and 1 atm pressure. The number of imaginary frequencies (IFs) obtained from frequency calculations confirmed the nature of all intermediates (no IF) and transition states (only one IF). All transition states were confirmed to connect corresponding reactants and products by intrinsic reaction coordinate calculations. The 3D molecular structures shown in this paper were drawn using the JIMP2 molecular visualizing and manipulating program [38]. We also evaluated the reliability of the $\omega\text{B97X-D}$ functional for this cobalt catalytic system, as well as the spin states of the structures in the reaction coordinates. The results are provided in the Supplementary Materials as Tables S1–S4.

4. Conclusions

In summary, our DFT study of the mechanistic insights into the hydrogenations of C=C bonds in hex-5-en-2-one, isoprene, and 4-vinylcyclohex-1-ene catalyzed by $(^{\text{Mes}}\text{CCC})\text{Co}$ complexes reveals that a Co dihydride complex **4'** is the real catalyst in the catalytic cycles. In all three hydrogenation reactions, the complex **3** with a PPh_3 ligand coordinated to Co is the resting state. The H_2 cleavages for the formations of C–H bonds in the final products are the turnover-limiting steps, with total free energy barriers of 19.2 ($3 \rightarrow \text{TS}_{8,4'}$), 21.3 ($3 \rightarrow \text{TS}_{15,4'}$), and 21.4 kcal/mol ($3 \rightarrow \text{TS}_{22,4'}$) in the hydrogenations of hex-5-en-2-one, isoprene, and 4-vinylcyclohex-1-ene, respectively. Our calculation results also indicate that the hydrogenation selectivity of different C=C bonds is dominated by the steric effect, while the hydrogenation selectivity of C=C and C=O bonds in the same compound could primarily be influenced by the electronic effect. In addition, the observed inhibition of the hydrogenation reactions by the excessive addition of PPh_3 could be explained by a free energy barrier of 15.8 kcal/mol for the dissociation of PPh_3 from **3**.

Supplementary Materials: The following are available online at <https://www.mdpi.com/2073-4344/11/2/168/s1>: Absolute and relative free energies of $^{\text{S}}8$ and $^{\text{S}}\text{TS}_{8,4'}$ (Table S1), $^{\text{S}}15$ and $^{\text{S}}\text{TS}_{15,4'}$ (Table S2), and $^{\text{S}}22$ and $^{\text{S}}\text{TS}_{22,4'}$ (Table S3) calculated by using different density functionals; Table S4: Absolute and relative free energies of singlet and triplet states of key intermediates and transition states.

Author Contributions: Conceptualization, Z.Z. and X.Y.; Methodology, Z.Z.; Writing—original draft, Z.Z.; Writing—review and editing, X.Y. All authors have read and agreed to the published version of the manuscript.

Funding: This work is supported by the National Natural Science Foundation of China (21873107, 21703256).

Data Availability Statement: Data is contained within the article or Supplementary Materials.

Conflicts of Interest: The authors declare no conflict of interest.

References

1. Verendel, J.J.; Pamies, O.; Dieguez, M.; Andersson, P.G. Asymmetric Hydrogenation of Olefins Using Chiral Crabtree-Type Catalysts: Scope and Limitations. *Chem. Rev.* **2014**, *114*, 2130–2169. [[CrossRef](#)]
2. Burgess, K.; Zhu, Y. Filling Gaps in Asymmetric Hydrogenation Methods for Acyclic Stereocontrol: Application to Chirons for Polyketide-Derived Natural Products. *Acc. Chem. Res.* **2011**, *45*, 1623–1636.
3. Church, T.L.; Andersson, P.G. Iridium catalysts for the asymmetric hydrogenation of olefins with nontraditional functional substituents. *Coord. Chem. Rev.* **2008**, *252*, 513–531. [[CrossRef](#)]
4. Roseblade, S.J.; Pfaltz, A. Iridium-Catalyzed Asymmetric Hydrogenation of Olefins. *Acc. Chem. Res.* **2007**, *40*, 1402–1411. [[CrossRef](#)] [[PubMed](#)]
5. Burgess, K.; Cui, X.H. Catalytic Homogeneous Asymmetric Hydrogenations of Largely Unfunctionalized Alkenes. *Chem. Rev.* **2005**, *105*, 3272–3296.
6. Hartwig, J.F. (Ed.) *Organotransition Metal Chemistry: From Bonding to Reactivity*; University Science Books: Sausalito, CA, USA, 2010.
7. Choi, J.; MacArthur, A.H.; Brookhart, M.; Goldman, A.S. Dehydrogenation and related reactions catalyzed by iridium pincer complexes. *Chem. Rev.* **2011**, *111*, 1761–1779. [[CrossRef](#)] [[PubMed](#)]
8. Wu, X.; Li, X.; Zanotti-Gerosa, A.; Pettman, A.; Liu, J.; Mills, A.J.; Xiao, J. Rh^{III}- and Ir^{III}-catalyzed asymmetric transfer hydrogenation of ketones in water. *Chem. Eur. J.* **2008**, *14*, 2209–2222. [[CrossRef](#)]
9. Etayo, P.; Vidal-Ferran, A. Rhodium-catalysed asymmetric hydrogenation as a valuable synthetic tool for the preparation of chiral drugs. *Chem. Soc. Rev.* **2013**, *42*, 728–754. [[CrossRef](#)]
10. Junge, H.; Loges, B.; Beller, M. Novel improved ruthenium catalysts for the generation of hydrogen from alcohols. *Chem. Commun.* **2007**, 522–524. [[CrossRef](#)]
11. Huff, C.A.; Kampf, J.W.; Sanford, M.S. Reversible carbon-carbon bond formation between carbonyl compounds and a ruthenium pincer complex. *Chem. Commun.* **2013**, *49*, 7147–7149. [[CrossRef](#)]
12. Nielsen, M.; Alberico, E.; Baumann, W.; Drexler, H.J.; Junge, H.; Gladiali, S.; Beller, M. Low-temperature aqueous-phase methanol dehydrogenation to hydrogen and carbon dioxide. *Nature* **2013**, *495*, 85–89. [[CrossRef](#)] [[PubMed](#)]
13. Dobreiner, G.E.; Crabtree, R.H. Dehydrogenation as a Substrate-Activating Strategy in Homogeneous Transition-Metal Catalysis. *Chem. Rev.* **2010**, *110*, 681–703. [[CrossRef](#)] [[PubMed](#)]
14. Chen, Q.A.; Ye, Z.S.; Duan, Y.; Zhou, Y.G. Homogeneous palladium-catalyzed asymmetric hydrogenation. *Chem. Soc. Rev.* **2013**, *42*, 497–511. [[CrossRef](#)] [[PubMed](#)]
15. Chirik, P.J. Iron- and Cobalt-Catalyzed Alkene Hydrogenation: Catalysis with Both Redox-Active and Strong Field Ligands. *Acc. Chem. Res.* **2015**, *48*, 1687–1695. [[CrossRef](#)]
16. Bart, S.C.; Lobkovsky, E.; Chirik, P.J. Preparation and Molecular and Electronic Structures of Iron(0) Dinitrogen and Silane Complexes and Their Application to Catalytic Hydrogenation and Hydrosilation. *J. Am. Chem. Soc.* **2004**, *126*, 13794–13807. [[CrossRef](#)]
17. Fong, H.; Peters, J.C. Hydricity of an Fe-H Species and Catalytic CO₂ Hydrogenation. *Inorg. Chem.* **2015**, *54*, 5124–5135. [[CrossRef](#)]
18. Liu, T.; Wang, X.; Hoffmann, C.; DuBois, D.L.; Bullock, R.M. Heterolytic cleavage of hydrogen by an iron hydrogenase model: An Fe-H...H-N dihydrogen bond characterized by neutron diffraction. *Angew. Chem. Int. Ed.* **2014**, *53*, 5300–5304. [[CrossRef](#)]
19. Archer, A.M.; Bouwkamp, M.W.; Cortez, M.P.; Lobkovsky, E.; Chirik, P.J. Arene Coordination in Bis(imino)pyridine Iron Complexes: Identification of Catalyst Deactivation Pathways in Iron-Catalyzed Hydrogenation and Hydrosilation. *Organometallics* **2006**, *25*, 4269–4278. [[CrossRef](#)]
20. Yu, R.P.; Darmon, J.M.; Hoyt, J.M.; Margulieux, G.W.; Turner, Z.R.; Chirik, P.J. High-Activity Iron Catalysts for the Hydrogenation of Hindered, Unfunctionalized Alkenes. *ACS Catal.* **2012**, *2*, 1760–1764. [[CrossRef](#)]
21. Knijnenburg, Q.; Horton, A.D.; Heijden, H.; Kooistra, T.M.; Hetterscheid, D.G.H.; Smits, J.M.M.; Bruin, B.; Budzelaar, P.H.M.; Gal, A.W. Olefin Hydrogenation Using Diimine Pyridine Complexes of Co and Rh. *J. Mol. Catal. A Chem.* **2005**, *232*, 151–159. [[CrossRef](#)]
22. Zhang, G.; Scott, B.L.; Hanson, S.K. Mild and Homogeneous Cobalt-Catalyzed Hydrogenation of C=C, C=O, and C=N Bonds. *Angew. Chem. Int. Ed.* **2012**, *51*, 12102–12106. [[CrossRef](#)] [[PubMed](#)]
23. Zhang, G.; Vasudevan, K.V.; Scott, B.L.; Hanson, S.K. Understanding the Mechanisms of Cobalt-Catalyzed Hydrogenation and Dehydrogenation Reactions. *J. Am. Chem. Soc.* **2013**, *135*, 8668–8681. [[CrossRef](#)] [[PubMed](#)]

24. Lin, T.P.; Peters, J.C. Boryl-Metal Bonds Facilitate Cobalt/Nickel-Catalyzed Olefin Hydrogenation. *J. Am. Chem. Soc.* **2014**, *136*, 13672–13683. [[CrossRef](#)] [[PubMed](#)]
25. Lin, T.P.; Peters, J.C. Boryl-Mediated Reversible H₂ Activation at Cobalt: Catalytic Hydrogenation, Dehydrogenation, and Transfer Hydrogenation. *J. Am. Chem. Soc.* **2013**, *135*, 15310–15313. [[CrossRef](#)]
26. Friedfeld, M.R.; Shevlin, M.; Margulieux, G.W.; Campeau, L.C.; Chirik, P.J. Cobalt-Catalyzed Enantioselective Hydrogenation of Minimally Functionalized Alkenes: Isotopic Labeling Provides Insight into the Origin of Stereoselectivity and Alkene Insertion Preferences. *J. Am. Chem. Soc.* **2016**, *138*, 3314–3324. [[CrossRef](#)] [[PubMed](#)]
27. Tokmic, K.; Markus, C.R.; Zhu, L.; Fout, A.R. Well-Defined Cobalt(I) Dihydrogen Catalyst: Experimental Evidence for a Co(I)/Co(III) Redox Process in Olefin Hydrogenation. *J. Am. Chem. Soc.* **2016**, *138*, 11907–11913. [[CrossRef](#)]
28. Tokmic, K.; Greer, R.B.; Zhu, L.; Fout, A.R. ¹³C NMR Signal Enhancement Using Parahydrogen-Induced Polarization Mediated by a Cobalt Hydrogenation Catalyst. *J. Am. Chem. Soc.* **2018**, *140*, 14844–14850. [[CrossRef](#)]
29. Tokmic, K.; Fout, A.R. Alkyne Semihydrogenation with a Well-Defined Nonclassical Co-H₂ Catalyst: A H₂ Spin on Isomerization and E-Selectivity. *J. Am. Chem. Soc.* **2016**, *138*, 13700–13705. [[CrossRef](#)]
30. Muhammad, S.R.; Nugent, J.W.; Tokmic, K.; Zhu, L.; Mahmoud, J.; Fout, A.R. Electronic Ligand Modifications on Cobalt Complexes and Their Application toward the Semi-Hydrogenation of Alkynes and Para-Hydrogenation of Alkenes. *Organometallics* **2019**, *38*, 3132–3138. [[CrossRef](#)]
31. Frisch, M.J.; Trucks, G.W.; Schlegel, H.B.; Scuseria, G.E.; Robb, M.A.; Cheeseman, J.R.; Scalmani, G.; Barone, V.; Mennucci, B.; Petersson, G.A.; et al. *Gaussian 09, Revision, C.01*; Gaussian, Inc.: Wallingford, CT, USA, 2010.
32. Chai, J.D.; Head-Gordon, M. Long-range corrected hybrid density functionals with damped atom-atom dispersion corrections. *Phys. Chem. Chem. Phys.* **2008**, *10*, 6615–6620. [[CrossRef](#)]
33. Hehre, W.J.; Ditchfield, R.; Pople, J.A. Self-Consistent Molecular Orbital Methods. XII. Further Extensions of Gaussian-Type Basis Sets for Use in Molecular Orbital Studies of Organic Molecules. *J. Chem. Phys.* **1972**, *56*, 2257–2261. [[CrossRef](#)]
34. Krishnan, R.; Binkley, J.S.; Seeger, R.; Pople, J.A. Self-consistent molecular orbital methods. XX. A basis set for correlated wave functions. *J. Chem. Phys.* **1980**, *72*, 650–654. [[CrossRef](#)]
35. Martin, J.M.L.; Sundermann, A. Correlation consistent valence basis sets for use with the Stuttgart-Dresden-Bonn relativistic effective core potentials: The atoms Ga-Kr and In-Xe. *J. Chem. Phys.* **2000**, *112*, 3408–3420. [[CrossRef](#)]
36. Tomasi, J.; Mennucci, B.; Cammi, R. Quantum Mechanical Continuum Solvation Models. *Chem. Rev.* **2005**, *105*, 2999–3093. [[CrossRef](#)]
37. Marenich, A.V.; Cramer, C.T.; Truhlar, D.G. Universal Solvation Model Based on Solute Electron Density and on a Continuum Model of the Solvent Defined by the Bulk Dielectric Constant and Atomic Surface Tensions. *J. Phys. Chem. B* **2009**, *113*, 6378–6396. [[CrossRef](#)]
38. Manson, J.; Webster, C.E.; Hall, M.B. *JIMP2, Version 0.091*; A Free Program for Visualizing and Manipulating Molecules; Texas A&M University: College Station, TX, USA, 2006.